

Enhanced Multi-level Features for Very High Resolution Remote Sensing Scene Classification

Chiranjibi Sitaula*, Sumesh KC, and Jagannath Aryal, *Member, IEEE*,

Abstract—Very high-resolution (VHR) remote sensing (RS) scene classification is a challenging task due to the higher inter-class similarity and intra-class variability problems. Recently, the existing deep learning (DL)-based methods have shown great promise in VHR RS scene classification. However, they still provide an unstable classification performance. To address such a problem, we, in this letter, propose a novel DL-based approach. For this, we devise an enhanced VHR attention module (EAM), followed by the atrous spatial pyramid pooling (ASPP) and global average pooling (GAP). This procedure imparts the enhanced features from the corresponding level. Then, the multi-level feature fusion is performed. Experimental results on two widely-used VHR RS datasets show that the proposed approach yields a competitive and stable/robust classification performance with the least standard deviation of 0.001. Further, the highest overall accuracies on the AID and the NWPU datasets are 95.39% and 93.04%, respectively.

Index Terms—Convolutional neural networks, feature extraction, machine learning, deep learning, remote sensing.

I. INTRODUCTION

REMOTE sensing (RS) scene classification using very high resolution (VHR) images, which is a source of spatial information, has attracted wider attention in robotics and earth observation. With the proliferation of such images, there has been rapid progress in VHR RS scene image interpretation tasks, such as scene classification, image retrieval, object detection, and semantic segmentation. Nevertheless, challenges such as complex spatial structures, diverse semantic categories, higher inter-class similarity, and intra-class variability have resulted in sub-optimal classification performance.

With the predominance of deep learning (DL)-based methods, particularly convolutional neural networks (CNNs) with recent advances, the classification performance of VHR RS scene images has been ground-breaking these days as in indoor/outdoor scene image classification [1], [2]. The DL-based methods that leverage transfer learning in this domain have been focused on either an end-to-end approach [3] or a two-step approach [4]. The end-to-end approach exploits the fine-tuning strategy and employs either the uni-modal-based multi-level feature fusion [3] or the ensemble approach [5]. Several works have been carried out in the literature using the end-to-end approach for the VHR RS scene classification. For example, Wang et al. [6] employed the attention recurrent convolutional network (ARCNet) for the VHR RS scene classification, which helped select the salient spatial regions sequentially. Furthermore, He et al. [7] designed a

skip-connected covariance (SCCov) network to classify the VHR RS scene images. The classification performance was improved based on the second-order information from the SCCov network. Considering the object relationship importance, Li et al. [8] established a DL model called object relationship reasoning CNN (ORRCNN), which adopts the scene and object-detection pipeline. Their work resulted in the overall improvement of the classification performance. Similarly, Wang et al. [3] developed a multi-level feature fusion (MLFF) module, which employs a novel adaptive channel dimension reduction approach and improved accuracy significantly. Furthermore, Li et al. [9] devised a multi-scale residual network with higher-order feature information to improve the classification performance. Following the efficacy of multi-scale information in scene classification problems, Wang et al. [10] recently devised the global-local two-stream architecture and significantly improved the VHR RS scene classification performance. Despite the significant improvement in the overall classification performance by this approach, it has unstable performance.

In the two-step approach, deep features are first extracted from the pre-trained DL models, also called transfer learning by feature extraction, and classified using a separate machine learning algorithm [4]. Few seminal works using this approach have been done compared to the end-to-end approach in the literature. For example, Weng et al. [4] extracted deep features using the AlexNet-like architecture pre-trained on the *ImageNet* and classified them using the extreme learning machine (ELM) classifier. Furthermore, Yu & Liu [11] extracted deep features from the VGG-16 and GoogleNet and classified them using the ELM classifier. Similarly, He et al. [12] extracted the deep features from the pre-trained CNN models (AlexNet and VGG-16), stacked them, and calculated the covariance matrix to achieve the complementary information. After that, such features were used to classify using the support vector machine (SVM) classifier. Furthermore, Sun et al. [13] developed an approach to represent the image using both deep and hand-crafted features, which were then encoded using well-established methods such as bag-of-visual-words (BoVW) and scale-invariant scale transform (SIFT) for the classification using the SVM classifier. The involvement of innovative deep feature extraction and the appropriate encoding steps improved the overall classification performance. The two-step approach has provided an encouraging result; however, they require the expertise of multiple algorithms to get maximum benefits and still provides an unstable performance.

The existing DL-based methods have produced an excellent overall classification performance; however, the results are still

C Sitaula (*Corresponding author), S KC, and J Aryal are with the Department of Infrastructure Engineering, The University of Melbourne, Parkville, VIC 3010.

unstable because of the limited/insufficient semantic information (features) extracted by them. The robustness/stability of the DL model could be maintained using an enhanced multi-level feature extraction procedure. To deal with this shortcoming, we propose a novel DL-based approach, which follows the enhanced multi-level feature extraction procedure. For this, our approach first devises an enhanced VHR attention module (EAM), which is based on the convolutional block attention module (CBAM) [14], to achieve rich discriminating salient information. This is further enhanced by the multi-scale information using the atrous spatial pyramid pooling (ASPP) [15] and global average pooling (GAP). In summary, the main **contributions** in this letter are as follows:

- 1) Develop and apply the EAM to attain the enriched salient information;
- 2) Achieve the multi-scale information using the ASPP over EAM-based features for the corresponding level, followed by the GAP and multi-level feature fusion; and
- 3) Show the superiority/validity of the proposed approach on two commonly-used VHR RS datasets through a comparative study with the state-of-the-art (SOTA) methods followed by an ablation study.

II. PROPOSED APPROACH

The proposed approach (Fig. 1) for high-level workflow has three major steps: Feature Extraction (Sec. II-A), EAM (Sec. II-B) and Feature Fusion (Sec. II-C).

A. Feature Extraction

We resort to the ResNet-50 model [16] for the feature extraction, as suggested by Wang et al. [3]. In the ResNet-50 model, same-sized feature maps generated from the layers are called stages. In total, there are five stages in this model. Among them, the last four stages are useful for VHR RS scene classification [3] as they jointly have the capability to achieve information from the basic to the higher level. So, we exploit only the last layers from each of the four stages, representing each level. We denote the features extracted from those layers as S_2 , S_3 , S_4 , and S_5 , which provides the number of channels as 256, 512, 1024, and 2048, respectively.

B. EAM

The proposed enhanced VHR attention module (EAM) has four main blocks: dimension reduction, upper, middle, and lower. The pipeline of the EAM is shown in Fig. 2.

1) *Dimension reduction block*: The uniform-sized tensors are pivotal to mitigate the risk of information bias provided by the higher-sized tensors as higher-sized tensors outweigh the lower-sized tensors during the concatenation-based feature fusion. To achieve the uniform-sized tensor, we perform the 1×1 convolution operation (refer to Eq. (1)) and feed it into the three blocks (upper, middle, and lower blocks).

$$I' = f^{1 \times 1}(I), \quad (1)$$

where $I' \in \mathbb{R}^{C' \times H \times W}$ ($C' \leq C$), which is obtained from the input tensor $I \in \mathbb{R}^{C \times H \times W}$ using the 2D convolution (f) with super-scripted kernel size of 1×1 .

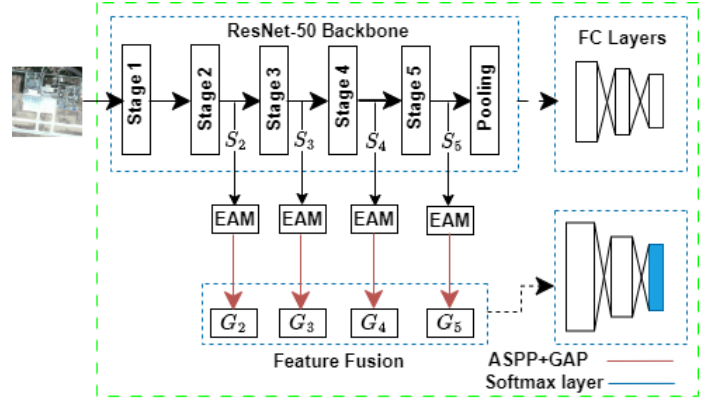


Fig. 1. High-level pipeline of the proposed approach. Note that S_2 , S_3 , S_4 , and S_5 denote the chosen layers from the second, third, fourth, and fifth stages, respectively as in [3].

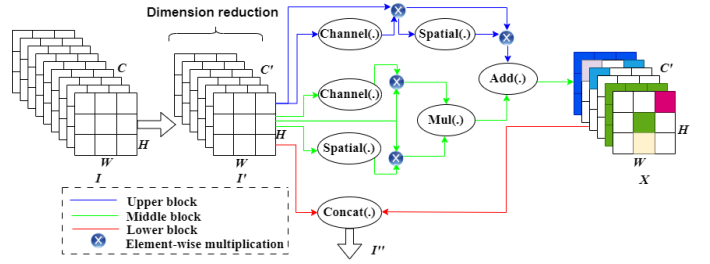


Fig. 2. Enhanced VHR attention module (EAM) used in our study.

2) *Upper block*: The upper block achieves the salient information from channel and spatial regions using the CBAM [14], which comprises two sequentially-arranged blocks, namely the channel attention block (Eq. (2)), and the spatial attention block (Eq. (3)).

$$F' = Channel(I') \otimes I', \quad (2)$$

$$F'' = Spatial(F') \otimes F', \quad (3)$$

where F' , F'' , and \otimes denote the output of channel attention block ($Channel(\cdot)$), spatial attention block ($Spatial(\cdot)$), and element-wise multiplication, respectively. As an example for the input tensor I' , the channel attention block ($Channel(I')$) uses max pooling ($MaxP(I')$) and average pooling ($AvgP(I')$) operations, and adds (+) them, followed by the one hidden-layered multi-layer perceptron (MLP) for both operations and then the *Sigmoid* activation (σ) on them (Eq. (4)).

$$Channel(I') = \sigma(MLP(AvgP(I') + MLP(MaxP(I')))) \quad (4)$$

Whereas, for F' , the spatial attention block ($Channel(F')$) employs the max pooling ($MaxP(F')$) and average pooling ($AvgP(F')$), with their concatenation ($;$), followed by the 2D convolution over 7×7 kernel size ($f^{7 \times 7}$) with the *Sigmoid* activation (Eq. (5)).

$$Spatial(F') = \sigma(f^{7 \times 7}([AvgP(F'); MaxP(F')]) \quad (5)$$

The sequential arrangement of channel and spatial attention blocks lacks the salient information that is obtained from the parallel arrangement, which is crucial complementary information for the separability of images. To this end, we add a middle block to complement the upper block, thereby producing complementary semantic information.

3) *Middle block*: Here, we combine the channel attention output (Eq. (6)) with spatial attention output (Eq. (7)) using the element-wise multiplicative operation (Eq. 8), followed by the addition operation with the upper block output (Eq. (9)). This helps combine the outputs obtained from the sequential attention block with the ones from the parallel attention block.

$$\lambda = \text{Channel}(I') \otimes I', \quad (6)$$

$$\beta = \text{Spatial}(I') \otimes I', \quad (7)$$

$$\delta = \text{Mul}(\lambda, \beta), \quad (8)$$

$$X = \text{Add}(F'', \delta), \quad (9)$$

where λ , β , δ , and X denote the output from channel attention, spatial attention, element-wise multiplication ($\text{Mult}(\cdot)$), and element-wise addition operation ($\text{Add}(\cdot)$), respectively.

4) *Lower block*: The lower block is designed to combine the convolutional features with the attention-based features obtained from the middle block (refer to Eq. (10)). Note that the simple concatenation operator is used to combine here.

$$I'' = \text{Concat}(I', X), \quad (10)$$

where I'' denotes the result obtained from the concatenation ($\text{Concat}(\cdot)$) of I' with X . Attention-based features alone are insufficient to discriminate the images accurately during classification, so it is essential to include convolutional features additionally for performance improvement [17]. To this end, this block combines the attention features obtained from the middle blocks with the convolutional features achieved from the dimension reduction block.

TABLE I

COMPARATIVE STUDY USING OVERALL CLASSIFICATION ACCURACY (%) \pm STANDARD DEVIATION ON THE AID DATASET. PLEASE NOTE THAT TR=TRAINING, TE=TESTING, AND BLUE-COLORED VALUES DENOTE THE HIGHEST PERFORMANCE, WHICH IS SIMILAR IN TABLES II AND III.

Method	Tr=50% Te=50%	Tr=20% Te=80%
ARCNet-VGG16 [6]	93.10 \pm 0.550	88.75 \pm 0.400
MSCP [12]	94.42 \pm 0.170	91.52 \pm 0.210
CNN+ELM [11]	94.58 \pm 0.250	92.32 \pm 0.410
LCPB [13]	91.33 \pm 0.360	87.68 \pm 0.250
LCPP [13]	93.12 \pm 0.280	90.96 \pm 0.330
ORRCNN [8]	92.00	86.42
ACR-MLFF [3]	95.06 \pm 0.330	92.73 \pm 0.120
MRHNet-50 [9]	95.06	91.14
Ours	95.39 \pm 0.001	93.14 \pm 0.003

C. Feature Fusion

Let $g: S'_i \rightarrow S''_i$, where S'_i and S''_i denote the input tensor extracted from the ResNet-50 and resultant output tensor achieved from the EAM (denoted by g function here) for the i^{th} layer (level), respectively. Note that $i \in \{2, \dots, 5\}$. Such features are further enhanced using the ASPP operations to achieve the multi-scale information [15] (Eq.(11)). Based on Chen et al. [15], we employ a kernel size of 1 with a dilation ratio of 1 and a kernel size of 3 with a dilation ratio of 6, 12, and 18 for the ASPP.

$$H_i = \text{ASPP}(S''_i), \quad (11)$$

where H_i denotes the features obtained from the ASPP operation of the i^{th} layer. Given that the ASPP produces tensors that need to be aggregated before fusion, we employ the global average pooling (GAP) operation, which not only provides the scale-invariant features but also preserves both minimum and maximum activation information during aggregation (Eq. (12)).

$$G_i = \text{GAP}(H_i), \quad (12)$$

where G_i denotes the features obtained from GAP operation for the corresponding i^{th} layer. Finally, such features from all four layers are fused using a simple concatenation-based feature fusion approach (Eq. (13)) and then classified into different classes using the *Softmax* layer.

$$F = [G_2; G_3; G_4; G_5], \quad (13)$$

where F represents the enhanced multi-level features, which are used for the classification.

III. EXPERIMENT AND ANALYSIS

In this section, we discuss dataset settings, implementation strategies, and experimental result analysis, followed by the ablation study.

A. Datasets

We perform our experiment on two commonly-used VHR RS datasets: Aerial Image Data Set (AID) [19], and NWPU-RESISC45 (NWPU) [20]. The AID contains a collection of 10,000 images divided into 30 classes. The number of images in each category varies from 220 to 420. Each image is 600×600 pixels in size, and the spatial resolution ranges from 0.5 to 8 m. Similarly, the NWPU is a larger RS dataset containing

TABLE II

COMPARATIVE STUDY USING VERALL CLASSIFICATION ACCURACY (%) \pm STANDARD DEVIATION ON THE NWPU DATASET.

Method	Tr=10% Te=90%	Tr=20% Te=80%
MSCP [12]	88.07 \pm 0.180	90.81 \pm 0.130
SCCov [7]	89.30 \pm 0.350	92.10 \pm 0.250
SKAL [10]	90.41 \pm 0.120	92.95 \pm 0.090
MRHNet-101 [18]	-	91.64
ACR-MLFF [3]	90.01 \pm 0.330	92.45 \pm 0.200
Ours	90.38 \pm 0.001	93.04 \pm 0.001

TABLE III
ABLATION STUDY USING OVERALL CLASSIFICATION ACCURACY (%) \pm STANDARD DEVIATION ON BOTH DATASETS.

Strategy	NWPU				AID			
	Tr=10%	Te=90%	Tr=20%	Te=80%	Tr=50%	Te=50%	Tr=20%	Te=80%
GAP	90.04 \pm 0.003		92.88 \pm 0.002		95.04 \pm 0.004		92.63 \pm 0.001	
ASPP + GAP	89.99 \pm 0.003		92.88 \pm 0.001		95.30 \pm 0.002		92.76 \pm 0.004	
EAM + GAP	89.52 \pm 0.004		92.64 \pm 0.002		94.70 \pm 0.003		92.02 \pm 0.004	
EAM + ASPP + GAP	90.38 \pm 0.001		93.04 \pm 0.001		95.39 \pm 0.001		93.14 \pm 0.003	

31,500 images distributed into 45 classes. Each image has the size of 256×256 pixels, and varying spatial resolution from 0.2 to 30 m.

For the evaluation, we design train:test splits using the standard method as in existing works [3], [9] for both datasets. For the AID dataset, we design two sets of five random train:test splits with a ratio of 50:50 and 20:80, respectively. Similarly, for the NWPU dataset, we prepare two sets of five random train:test splits with a ratio of 10:90 and 20:80, respectively. We report the averaged overall classification performance over five splits with the standard deviation for each set on both datasets.

B. Implementation

All experiments are performed using NVIDIA GeForce RTX 3070 Ti Laptop GPU with the Keras under Tensorflow package [21] in Python. We employ the *Adam* optimizer, where we set the weight decay penalty and *batch_size* to 1×10^{-4} and 16, respectively. The learning rate and the number of epochs are set to 3×10^{-3} and 50, respectively. We apply a horizontal flip with random cropping and shuffling operations for data augmentation.

C. Results and Discussion

1) *Comparison with the SOTA methods:* We compared the overall classification accuracy of our proposed approach with the SOTA methods on both the datasets. The results are presented in Tables I and II for the AID and NWPU datasets, respectively. From Table I, we observe that our approach outperforms the recent methods for 50:50 and 20:80 settings with the stable classification accuracy of 95.39% (0.33% higher than the best-performing method (ACR-MLFF [3])), and 93.14% (0.41% higher than the best-performing method (ACR-MLFF [3])), respectively. We also observe that it shows stable performance with the lowest standard deviation of 0.001 for the 50:50 setting and 0.003 for the 20:80 setting.

From Table II, we notice that our approach yields prominent classification accuracy of 90.38% for the 10:90 setting (0.03% lower than the best-performing method (SKAL [10])) and 93.04% for the 20:80 setting (0.09% higher than the best-performing method (SKAL [10])). Although the proposed approach imparts a slightly lower accuracy than the best-performing method for the 10:90 setting on the NWPU, it produces a stable and robust performance with the lowest standard deviation (0.001 for both the 10:90 and 20:80 settings).

2) *Ablation study:* To understand the role of EAM, ASPP, and GAP on all four layers, we analyse the performance of their four sequential combination strategies: GAP, ASPP+GAP, EAM+GAP, and EAM+ASPP+GAP. Note that GAP is used in every combination to achieve the final aggregated results. The results are presented in Table III. From Table III, we find that the sequential combination of three components (EAM+ASPP+GAP) provides more stable and improved performance compared to the remaining strategies. This result is attributed to the joint involvement of all three sequential components.

IV. CONCLUSION

In this letter, we proposed a novel DL-based approach using an enhanced multi-level feature extraction procedure to classify VHR RS images. Our approach outperforms with a stable classification performance with the highest accuracy of 95.39% on the AID and 93.04% on the NWPU datasets, where both of them have the least standard deviation (0.001). For future work, we recommend working on the proposed EAM with various pre-trained DL models (e.g., VGG-16, Xception, EfficientNet) on such datasets. Additionally, the potentiality of the ASPP with the EAM could be explored to boost the classification using different publicly available and benchmark datasets.

REFERENCES

- [1] C. Sitaula, Y. Xiang, S. Aryal, and X. Lu, "Scene image representation by foreground, background and hybrid features," *Expert Systems with Applications*, vol. 182, p. 115285, 2021.
- [2] C. Sitaula, T. B. Shahi, F. Marzbanrad, and J. Aryal, "Recent advances in scene image representation and classification," *Multimedia Tools and Applications*, 2023. in press.
- [3] X. Wang, L. Duan, A. Shi, and H. Zhou, "Multilevel feature fusion networks with adaptive channel dimensionality reduction for remote sensing scene classification," *IEEE Geoscience and Remote Sensing Letters*, vol. 19, pp. 1–5, 2022.
- [4] Q. Weng, Z. Mao, J. Lin, and W. Guo, "Land-Use Classification via Extreme Learning Classifier Based on Deep Convolutional Features," *IEEE Geoscience and Remote Sensing Letters*, vol. 14, pp. 704–708, 5 2017.
- [5] G. J. Scott, K. C. Hagan, R. A. Marcum, J. A. Hurt, D. T. Anderson, and C. H. Davis, "Enhanced fusion of deep neural networks for classification of benchmark high-resolution image data sets," *IEEE Geoscience and Remote Sensing Letters*, vol. 15, pp. 1451–1455, 9 2018.
- [6] Q. Wang, S. Liu, J. Chanussot, and X. Li, "Scene classification with recurrent attention of vhr remote sensing images," *IEEE Transactions on Geoscience and Remote Sensing*, vol. 57, no. 2, pp. 1155–1167, 2018.
- [7] N. He, L. Fang, S. Li, J. Plaza, and A. Plaza, "Skip-connected covariance network for remote sensing scene classification," *IEEE transactions on neural networks and learning systems*, vol. 31, no. 5, pp. 1461–1474, 2019.

- [8] Z. Li, Q. Wu, B. Cheng, L. Cao, and H. Yang, "Remote sensing image scene classification based on object relationship reasoning cnn," *IEEE Geoscience and Remote Sensing Letters*, vol. 19, pp. 1–5, 2022.
- [9] C. Li, Y. Zhuang, W. Liu, S. Dong, H. Du, H. Chen, and B. Zhao, "Effective multiscale residual network with high-order feature representation for optical remote sensing scene classification," *IEEE Geoscience and Remote Sensing Letters*, vol. 19, pp. 1–5, 2022.
- [10] Q. Wang, W. Huang, Z. Xiong, and X. Li, "Looking closer at the scene: Multiscale representation learning for remote sensing image scene classification," *IEEE Transactions on Neural Networks and Learning Systems*, vol. 33, no. 4, pp. 1414–1428, 2022.
- [11] Y. Yu and F. Liu, "A Two-Stream Deep Fusion Framework for High-Resolution Aerial Scene Classification," *Computational Intelligence and Neuroscience*, vol. 2018, 2018.
- [12] N. He, L. Fang, S. Li, A. Plaza, and J. Plaza, "Remote sensing scene classification using multilayer stacked covariance pooling," *IEEE Transactions on Geoscience and Remote Sensing*, vol. 56, no. 12, pp. 6899–6910, 2018.
- [13] X. Sun, Q. Zhu, and Q. Qin, "A multi-level convolution pyramid semantic fusion framework for high-resolution remote sensing image scene classification and annotation," *IEEE Access*, vol. 9, pp. 18195–18208, 2021.
- [14] S. Woo, J. Park, J.-Y. Lee, and I. S. Kweon, "Cbam: Convolutional block attention module," in *Proc. of the European conference on computer vision (ECCV)*, pp. 3–19, 2018.
- [15] L.-C. Chen, Y. Zhu, G. Papandreou, F. Schroff, and H. Adam, "Encoder-decoder with atrous separable convolution for semantic image segmentation," in *Proc. of the European conference on computer vision*, pp. 801–818, 2018.
- [16] K. He, X. Zhang, S. Ren, and J. Sun, "Deep residual learning for image recognition," in *Proc. of the IEEE conference on computer vision and pattern recognition*, pp. 770–778, 2016.
- [17] C. Sitaula and M. B. Hossain, "Attention-based vgg-16 model for covid-19 chest x-ray image classification," *Applied Intelligence*, vol. 51, pp. 2850–2863, 2021.
- [18] C. Li, Y. Zhuang, W. Liu, S. Dong, H. Du, H. Chen, and B. Zhao, "Effective multiscale residual network with high-order feature representation for optical remote sensing scene classification," *IEEE Geoscience and Remote Sensing Letters*, vol. 19, pp. 1–5, 2022.
- [19] G.-S. Xia, J. Hu, F. Hu, B. Shi, X. Bai, Y. Zhong, L. Zhang, and X. Lu, "Aid: A benchmark data set for performance evaluation of aerial scene classification," *IEEE Transactions on Geoscience and Remote Sensing*, vol. 55, no. 7, pp. 3965–3981, 2017.
- [20] G. Cheng, J. Han, and X. Lu, "Remote sensing image scene classification: Benchmark and state of the art," *Proceedings of the IEEE*, vol. 105, no. 10, pp. 1865–1883, 2017.
- [21] M. Abadi, P. Barham, J. Chen, Z. Chen, A. Davis, J. Dean, M. Devin, S. Ghemawat, G. Irving, M. Isard, *et al.*, "Tensorflow: a system for large-scale machine learning," in *Osd*, vol. 16, pp. 265–283, Savannah, GA, USA, 2016.